arXiv:1611.04316v2 [cond-mat.mtrl-sci] 23 Nov 2016

Data Mining for 3D Organic Dirac Materials: Focus on Space Group #19

R. Matthias Geilhufe[1],* Stanislav S. Borysov[1], Adrien Bouhon[2], and Alexander V. Balatsky[1,3]
[1] *Nordita, Center for Quantum Materials, KTH Royal Institute of Technology and Stockholm University, Roslagstullsbacken 23, SE-106 91 Stockholm, Sweden*
[2] *Department of Physics and Astronomy, Uppsala University, Box 516, SE-751 20 Uppsala, Sweden*
[3] *Institute for Materials Science, Los Alamos National Laboratory, Los Alamos, NM 87545, USA*
(Dated: November 24, 2016)

We combined the group theory and data mining approach within the Organic Materials Database that leads to the prediction of stable Dirac-point nodes within the electronic band structure of 3-dimensional organic crystals. We find a particular space group $P2_12_12_1$ (#19) that is conducive to the Dirac nodes formation. We prove that nodes are a consequence of the orthorhombic crystal structure. Within the electronic band structure, two different kinds of nodes can be distinguished: 8-fold degenerate Dirac nodes protected by the crystalline symmetry and 4-fold degenerate Dirac nodes protected by band topology. Mining the Organic Materials Database, we present band structure calculations and symmetry analysis for 6 previously synthesized organic materials. In all these materials, the Dirac nodes are well separated within the energy and located near the Fermi surface, which opens up a possibility for their direct experimental observation.

Recently, we have witnessed growing interest in the community in Dirac materials where the low-energy excitations behave as massless Dirac fermions [1]. Among the most prominent examples are the two-dimensional material graphene [2], the surface of bulk topological insulators [3] like $Pb_xSn_{1-x}Te$ [4–6], Dirac-line materials [7–11] and Weyl semimetals like TaAs [12, 13]. To date, the strong focus within electronic Dirac materials lies in the inorganic crystals. The class of organic crystals remains rather unexplored and only a few Dirac materials are known. One prominent example is the quasi 2-dimensional charge transfer salt α-(BEDT-TTF)$_2$I$_3$ which shows a tilted Dirac cone located at the Fermi energy under high pressure [14, 15]. Organic crystals offer a high potential for technological applications due to low production costs, elastic properties (flexible electronics) and the opportunity to build large-area devices [16–20]. We therefore will focus on exploring the space of organic materials with the specific goal of identifying Dirac materials.

Since the crystal structure plays a crucial role for hosting Dirac nodes, attempts of identifying organic Dirac materials so far are mainly based on variations of already known Dirac materials. In two dimensions, this can be done by starting with the graphene structure and replacing the carbon atoms by more complex organic molecules [21]. A similar strategy was also discussed with respect to α-(BEDT-TTF)$_2$I$_3$ [22, 23]. To go beyond this approach, we adopt a new strategy for the search of Dirac nodes in the class of 3-dimensional organic crystals. We performed a data mining study on the basis of about 5000 electronic Kohn-Sham band structures calculated using Density Functional Theory (DFT) [24–26] and stored within the Organic Materials Database (OMDB) [27], where we looked for *isolated* linear crossings, i.e., no other bands can be found besides the crossing withing the corresponding energy range. Although all considered organic materials were previously synthesized, little attention has been paid to the electronic structure for most of them so far.

To achieve stable Dirac points within the electronic structure, symmetry or topological protection needs to be present. In this connection, crystals with non-symmorphic space groups have been widely discussed [28–30] where the key role is played by high-dimensional irreducible representations at the Brillouin zone boundary. As a consequence of the Wigner-Eckart theorem, the degeneracy of an electronic state is equal to the dimension of an irreducible representation. In the context of crystals, these degeneracies were discussed in great detail during the 1960s [31–33]. Recently, with a reinterpretation, degenerate electronic states in crystals again attracted attention as a host to unconventional fermions as low-energy excitation [34]. There is also a second opportunity of hosting Dirac crossing as accidental crossings [35], which are protected by band topology. Such crossings can be found e.g. in crystals with the monoclinic space group $P2_1/c$ (#14) [7, 36]. In crystals with this space group, electronic energy bands are sticking together in groups of four bands. As reported in Ref. [7], for each of these groups three topologically different orderings of electronic states can be found at the Γ-point within the Brillouin zone—a trivial phase and two different line-node phases. Within the space group $P2_12_12_1$ (#19), an almost similar situation is present, with the difference that at least one crossing has to occur along one of the paths $\overline{\Gamma X}$, $\overline{\Gamma Y}$ or $\overline{\Gamma Z}$ within the Brillouin zone. This group will be discussed below in Results.

In this paper, we report results of a combined study using abstract group theory and data mining within the Organic Materials Database (OMDB) [27]. We point out the first real material examples in the class of 3-dimensional organic crystals hosting isolated Dirac nodes in the electronic structure:

$C_6H_7ClO_3$ [37], $C_{10}H_{10}Br_2Cl_3NO_2$ [38], $C_{12}H_{13}NO_2$ [39], $C_{13}H_{12}N_2O$ [40], $C_9H_{10}F_3NO$ [41], and $C_{10}H_{12}BrNO$ [42]. It will be shown that the found Dirac nodes are a consequence of the orthorhombic crystal structure of the space group $P2_12_12_1$ (#19). Within the band structure of the materials, two different kinds of nodes can be distinguished: 8-fold degenerate Dirac nodes protected by the crystalline symmetry and 4-fold degenerate tilted Dirac nodes protected by the band topology.

RESULTS

Data mining and ab initio calculations

As reported in Ref. [27], most 3-dimensional organic crystals are insulating. However, the doping of organic materials is extensively studied, opening the opportunity of shifting the Fermi level into the valence band (p-doping) or conduction band (n-doping) [16]. Therefore, we searched for isolated linear crossings in a neighborhood of 1 eV above the lowest unoccupied electronic state and below the highest occupied electronic state within the Kohn-Sham band structures stored in the OMDB by explicitly focusing our attention to materials with the space group $P2_12_12_1$ (#19). For the 6 most promising structures tabulated in Table I, additional refined DFT calculations were performed (see Methods for more details).

As a representative, we further concentrate on the discussion for the material $C_6H_7ClO_3$ (the electronic and molecular structures for the other 6 materials can be found in the supplementary material). The orthorhombic crystallographic unit cell is build up of four copies of $C_6H_7ClO_3$ molecules as shown in Fig. 1b. The calculated band structure along several high symmetry paths within the Brillouin zone (Fig. 1a) is plotted in Fig. 1d. The isolated linear crossings occur at the high-symmetry point R (green dashed circles in Fig. 1d) as well as along the high-symmetry path $\overline{\Gamma X}$ (red dotted circles in Fig. 1d). A picture of the linear energy dispersion within the $\vec{b}_2$-$\vec{b}_3$-plane within reciprocal space in the vicinity of the R-point can be seen in Fig. 1c. The linear crossings are well separated within the energy and as a consequence the electronic density of states grows quadratically with the energy in the vicinity of the 3D Dirac crossing ($n(E) \sim E^{d-1}$ [1]) as can be seen in Fig. 1d.

However, to justify the claim of the found materials being Dirac materials, a protection of the crossings by crystalline symmetry is necessary. Indeed we do find the crossings forming Dirac nodes in the spectra, their nature is investigated and explained in the framework of group theory below.

TABLE I: **Data-mined organic Dirac materials with the space group #19.** The first four materials show crossings in the valence band, the latter two have crossings in the conduction band. References to papers where the synthesis of the materials was reported are given in the last column.

#	OMDB ID	COD ID	sum formula	ref.
1	**3407**	**1504134**	$C_6H_7ClO_3$	[37]
2	**4071**	**1503207**	$C_{10}H_{10}Br_2Cl_3NO_2$	[38]
3	**3180**	**1506714**	$C_{12}H_{13}NO_2$	[39]
4	**5010**	**7153350**	$C_{13}H_{12}N_2O$	[40]
5	**3617**	**1506293**	$C_9H_{10}F_3NO$	[41]
6	**690**	**4066669**	$C_{10}H_{12}BrNO$	[42]

Group theory analysis

The space group $P2_12_12_1$ (#19) itself (hereinafter denoted by $\mathcal{G}$) is an infinite group having the group of pure translations $\mathcal{T}$ as an infinite, normal and Abelian subgroup. The point group of the lattice $\mathcal{G}_0$, i.e., the group of all rotational parts of the space group elements is given by 222 (D_2). The factor group $\mathcal{G}/\mathcal{T}$ is isomorphic to 222 and the coset representatives are given by

$$T_1 = (E, 0, 0, 0), \quad (1)$$
$$T_2 = (C_{2x}, 1/2, 1/2, 0), \quad (2)$$
$$T_3 = (C_{2y}, 0, 1/2, 1/2), \quad (3)$$
$$T_4 = (C_{2z}, 1/2, 0, 1/2). \quad (4)$$

Here, E denotes the identity element and C_{2x}, C_{2y} and C_{2z} denote two-fold rotations (rotations by 180°) about the Cartesian x-, y- and z-axis, respectively. In general, since $\mathcal{G}$ is an infinite group, it has infinitely many irreducible representations. However, due to the special structure of space groups they can be indexed by the combined index $(\vec{k}, p)$, where $\vec{k}$ denotes a vector in reciprocal space and p denotes an additional index running over all the allowed representations at $\vec{k}$. A degeneracy of a state with energy $E(\vec{k})$ can be expected when the associated irreducible representation $\Gamma^p_{\vec{k}}$ has dimension $d > 1$ or when pairs of complex conjugate representations are present. Such a degeneracy is denoted as "protected by the crystalline symmetry". At the R point within the Brillouin zone, the physically-irreducible representation is four dimensional [43]. Additional spin-degeneracy leads to an 8-fold degenerate linear crossing. Such crossings were recently referred to as double Dirac crossings [44]. Within the band structure in Fig. 1d, these crossings are highlighted by green dashed circles.

At the Γ point, the group of the $\vec{k}$-vector [32] is given by the whole space group. Each of the eigenstates is one-fold degenerate and belongs to one of the irreducible representations listed in Table IIa (spin degeneracy is omitted for the moment). As soon as one moves slightly away from the Γ point, for instance on the path $\overline{\Gamma X}$, the little

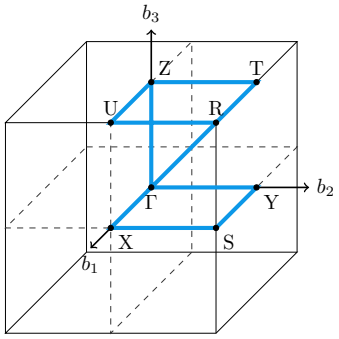

(a) Brillouin zone path for band structure calculation in Fig. 1d

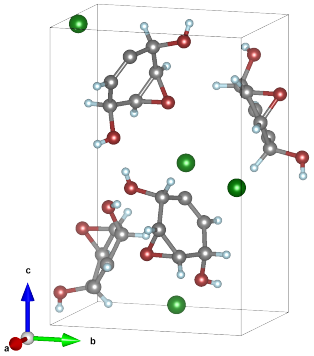

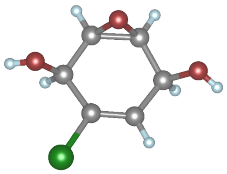

(b) Orthorhombic unit cell and single molecule of $C_6H_7ClO_3$. Grey denotes carbon, red oxygen, blue hydrogen and green chlorine

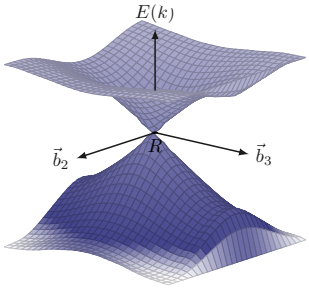

(c) Energy dispersion in $\vec{b}_2$-$\vec{b}_3$-plane around the R point

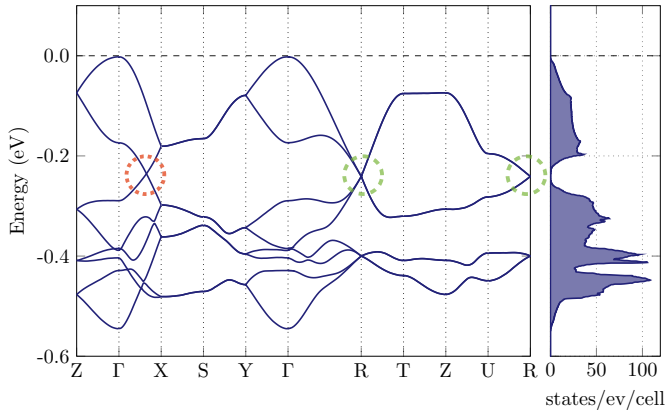

(d) Band structure and density of states. Crossings highlighted in green circles are 8-fold degenerate Dirac-points protected by crystalline symmetry and crossings in red circles are 4-fold degenerate Dirac points protected by band topology

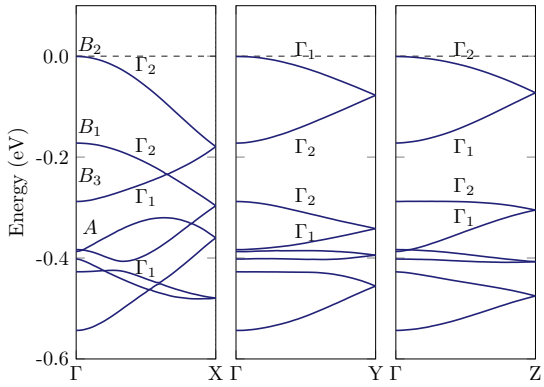

(e) Energy dispersion along $\overline{\Gamma X}$, $\overline{\Gamma Y}$, $\overline{\Gamma Z}$ and irreducible representations

FIG. 1: **Crystal structure and electronic structure of the orthorhombic organic crystal $C_6H_7ClO_3$.**

group of the $\vec{k}$-vector only contains the elements T_1 and T_2. Hence, the bands will be classified by their transformation behavior with respect to the two-fold rotation, namely even (Γ_1) or odd (Γ_2). Every state at X transforms as the 2-dimensional irreducible representation E illustrated in Table IIc. Moving towards X and coming from $\overline{\Gamma X}$ bands of character Γ_1 and Γ_2 have to merge pairwise. In general, bands can only cross (accidental crossings) when they belong to different irreducible representations [35]. Otherwise they will hybridize and form a spectral gap. Clearly, a similar consideration holds along $\overline{\Gamma Y}$ and $\overline{\Gamma Z}$. Taking into account all possible permutations of the four irreducible representations at Γ as well as the possible connections to X, Y and Z, it can be verified that at least one crossing can be found along one of the 3 paths. Taking into account the C_2 rotation symmetry, a second copy of the crossing along the path $\overline{\Gamma(-X)}$ can be found within the Brillouin zone. Furthermore, as soon as one slightly departs from one of the 3 paths towards the interior of the Brillouin zone, none of the symmetries is kept and only the identity element T_1 is present. Hence, there is no reason to protect the crossing at any point that is not lying on one of the 3 paths and

TABLE II: **Character tables and compatibility relations.**

(a) 222 (D_2)

	E	C_{2x}	C_{2y}	C_{2z}	$\{E, C_{2x}\}$	$\{E, C_{2y}\}$	$\{E, C_{2z}\}$
A	1	1	1	1	Γ_1	Γ_1	Γ_1
B_1	1	-1	-1	1	Γ_2	Γ_2	Γ_1
B_2	1	-1	1	-1	Γ_2	Γ_1	Γ_2
B_3	1	1	-1	-1	Γ_1	Γ_2	Γ_2

(b) 2 (C_2).

	E	C_2
Γ_1	1	1
Γ_2	1	-1

(c) $P2_12_12_1$ at X, Y and Z

	T_1	T_2	T_3	T_4
E	2	0	0	0

the crossing itself is a Dirac point. Hence, by including spin-degeneracy, this crossing is 4-fold degenerate. Furthermore, it is possible to show that the R point carries a spin-polarized Chern number of $C_s = +2$ which, by the Nielsen-Ninomiya theorem [45, 46], guarantees the existence of other degeneracies with a total canceling charge of -2. Thus, the two Dirac points must each carry a topological charge $C_s = -1$ [47].

In the present case of $C_6H_7ClO_3$, the topologically protected crossing can be found along the path ΓX, as can be verified from Fig. 1d and Fig. 1e. In Fig. 1d, the topologically protected crossing is highlighted by a red dotted circle. As can be seen, the four interesting bands below the Fermi level have the ordering A, B_3, B_1, B_2. Bands originating from A and B_1 and from B_3 and B_2 are merging pairwise at X for the above discussed reason. As a consequence, a crossing of bands originating from B_3 and B_1 can be observed (see Fig. 1e).

DISCUSSION

Within the paper, we presented the first 6 predicted compounds for 3-dimensional organic crystals hosting Dirac crossings. All 6 materials were synthesized before, so we encourage direct experimental verification of the results presented here. Within respective band structures, we identified 8-fold degenerate Dirac nodes at the R point in the Brillouin zone together with 4-fold degenerate topologically protected Dirac points along the high-symmetry path $\overline{\Gamma X}$. The crossings are well separated in energy due to the flat electronic bands of organic crystals and potentially accessible via doping or gating. In comparison to inorganic materials, the spatially sparse unit cells of organic materials characterized by van der Waals bonding between large molecules leads to an electronic structure characterized by blocks of well separated flat bands. This particular property also increases our chances of finding isolated topologically protected crossings. We expect that more organic Dirac materials will be reported elsewhere with growth of the OMDB database. Furthermore, the slope of the crossings is usually much smaller then for similar inorganic crystals leading to potential applications as slow Dirac materials [48].

METHODS

Materials data and data mining. For the data mining study, Kohn-Sham band structures for 3-dimensional organic crystals where considered which are stored within the organic materials database (OMDB) [27] (`http://omdb.diracmaterials.org`). The database itself contains about 5000 materials at the current stage. As a "hard" search criteria, we were looking for tiny energy gaps of the size of less than 0.01 eV as illustrated in Fig. 2. This choice assures detecting isolated Dirac crossings and, furthermore, introduces a numerical tolerance since the band structure calculations were performed along a discrete mesh. In a second step and as a "soft" search criteria, we applied a pattern matching algorithm based on the moving window approach to range selected band structures according to their similarity to a linear crossing pattern by choosing the root mean square error as a similarity measure.

Electronic structure calculations. Having found a subset of perspective materials, refined electronic structure calculations were performed in the framework of the density functional theory [24–26] by applying a pseudopotential projector augmented-wave method [49–52], as implemented in the Vienna Ab initio Simulation Package (VASP) [53–56] and the Quantum ESPRESSO code [57]. The exchange-correlation functional was approximated by the generalized gradient approximation according to Perdew, Burke and Ernzerhof [58]. The structural information were taken from the Crystallography Open Database (COD) [59–63] and transformed into capable input files by applying the Pymatgen package [64].

Within VASP, the precision flag was set to "normal" meaning that the energy cut-off is given by the maximum of the specified maxima for the cut-off energies within the POTCAR files (for example, for carbon this value is given by 400 eV). The calculations were performed spin-polarized but without spin-orbit coupling. For the integration in $\vec{k}$-space, a $6 \times 6 \times 6$ Γ-centred mesh according to Monkhorst and Pack [65] was chosen during the self-consistent cycle. A structural optimization was performed by allowing the ionic positions, the cell shape and the cell volume to change (ISIF = 3). Quantum ESPRESSO was applied to estimate the associated irreducible representations of the energy levels within the band structure. The cut-off energy for the wave function was chosen to be 48 Ry and the cut-off energy for the charge density and the potentials was chosen to be 316 Ry. Optimized structures from the VASP calculations were used. The calculated band structures using

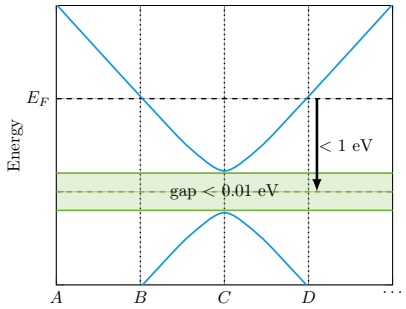

FIG. 2: **Illustration of search criteria for spectral gaps close to the Fermi level.**

VASP and Quantum ESPRESSO are in perfect agreement.

ACKNOWLEDGEMENTS

The work at Los Alamos is supported by the US Department of Energy, BES E3B7. Furthermore, the work was supported by the Swedish Research Council Grant No. 638-2013-9243, the Knut and Alice Wallenberg Foundation, and the European Research Council under the European Unions Seventh Framework Program (FP/2207-2013)/ERC Grant Agreement No. DM-321031. The authors acknowledge computational resources from the Max Planck Institute of Microstructure Physics in Halle (Germany) and the Swedish National Infrastructure for Computing (SNIC) at the National Supercomputer Centre at Linköping University.

EXTENDED FIGURES

In the following, the band structures and molecular structures of the mined materials are presented which were not discussed in the paper so far. The materials $C_{10}H_{10}Br_2Cl_3NO_2$ [38], $C_{12}H_{13}NO_2$ [39], and $C_{13}H_{12}N_2O$ [40] contain the above mentioned Dirac crossings in the valence band close to the highest occupied electronic state and are plotted in Fig. 3. The distance of the crossing to the Fermi-level is in the range of 100-200 meV. Within the materials $C_9H_{10}F_3NO$ [41] and $C_{10}H_{12}BrNO$ [42], similar crossings can be found in the conduction band. The distance of the crossing to the lowest unoccupied state is about 200 meV, as can be seen in Fig. 4

* Geilhufe@kth.se

[1] T. Wehling, A. M. Black-Schaffer, and A. V. Balatsky, Advances in Physics **63**, 1 (2014).
[2] D. Abergel, V. Apalkov, J. Berashevich, K. Ziegler, and T. Chakraborty, Advances in Physics **59**, 261 (2010).
[3] L. Fu, C. L. Kane, and E. J. Mele, Physical Review Letters **98**, 106803 (2007).
[4] Y. Tanaka, Z. Ren, T. Sato, K. Nakayama, S. Souma, T. Takahashi, K. Segawa, and Y. Ando, Nature Physics **8**, 800 (2012).
[5] M. Geilhufe, S. K. Nayak, S. Thomas, M. Däne, G. S. Tripathi, P. Entel, W. Hergert, and A. Ernst, Physical Review B **92**, 235203 (2015).
[6] T. H. Hsieh, H. Lin, J. Liu, W. Duan, A. Bansil, and L. Fu, Nature communications **3**, 982 (2012).
[7] R. M. Geilhufe, A. Bouhon, S. S. Borysov, and A. V. Balatsky, arXiv preprint arXiv:1610.07815 (2016).
[8] Y. Kim, B. J. Wieder, C. L. Kane, and A. M. Rappe, Phys. Rev. Lett. **115**, 036806 (2015).
[9] R. Yu, H. Weng, Z. Fang, X. Dai, and X. Hu, Phys. Rev. Lett. **115**, 036807 (2015).
[10] A. Yamakage, Y. Yamakawa, Y. Tanaka, and Y. Okamoto, Journal of the Physical Society of Japan **85**, 013708 (2016).
[11] H. Weng, Y. Liang, Q. Xu, R. Yu, Z. Fang, X. Dai, and Y. Kawazoe, Phys. Rev. B **92**, 045108 (2015).
[12] S.-Y. Xu, I. Belopolski, N. Alidoust, M. Neupane, G. Bian, C. Zhang, R. Sankar, G. Chang, Z. Yuan, C.-C. Lee, *et al.*, Science **349**, 613 (2015).
[13] B. Lv, H. Weng, B. Fu, X. Wang, H. Miao, J. Ma, P. Richard, X. Huang, L. Zhao, G. Chen, *et al.*, Physical Review X **5**, 031013 (2015).
[14] N. Tajima, M. Tamura, Y. Nishio, K. Kajita, and Y. Iye, Journal of the Physical Society of Japan **69**, 543 (2000).
[15] S. Katayama, A. Kobayashi, and Y. Suzumura, Journal of the Physical Society of Japan **75**, 054705 (2006).
[16] B. Lüssem, M. Riede, and K. Leo, physica status solidi (a) **210**, 9 (2013).
[17] S. R. Forrest and M. E. Thompson, Chemical Reviews **107**, 923 (2007).
[18] H. Klauk, *Organic electronics: materials, manufacturing, and applications* (John Wiley & Sons, 2006).
[19] T. W. Kelley, P. F. Baude, C. Gerlach, D. E. Ender, D. Muyres, M. A. Haase, D. E. Vogel, and S. D. Theiss, Chemistry of Materials **16**, 4413 (2004).
[20] J. M. Shaw and P. F. Seidler, IBM Journal of Research and Development **45**, 3 (2001).
[21] Z. Wang, N. Su, and F. Liu, Nano letters **13**, 2842 (2013).
[22] T. Choji, A. Kobayashi, and Y. Suzumura, Journal of the Physical Society of Japan **80**, 074712 (2011).
[23] T. Morinari and Y. Suzumura, Journal of the Physical Society of Japan **83**, 094701 (2014).
[24] P. Hohenberg and W. Kohn, Physical Review **136**, B864 (1964).
[25] W. Kohn and L. J. Sham, Physical Review **140**, A1133 (1965).
[26] R. O. Jones, Reviews of Modern Physics **87**, 897 (2015).
[27] S. S. Borysov, R. M. Geilhufe, and A. V. Balatsky, (2016).
[28] S. M. Young and C. L. Kane, Phys. Rev. Lett. **115**, 126803 (2015).
[29] L. M. Schoop, M. N. Ali, C. Straßer, V. Duppel, S. S. Parkin, B. V. Lotsch, and C. R. Ast, arXiv preprint arXiv:1509.00861 (2015).
[30] B.-J. Yang, T. A. Bojesen, T. Morimoto, and A. Furusaki, arXiv preprint arXiv:1604.00843 (2016).
[31] J. Zak, Journal of Mathematical Physics **1**, 165 (1960).
[32] J. F. Cornwell, *Group theory and electronic energy bands in solids*, Vol. 10 (North-Holland Pub. Co., 1969).
[33] C. Bradley and A. P. Cracknell, *The Mathematical Theory of Symmetry in Solids: Representation Theory for Points Groups and Space Groups* (Clarendon Press, 1972).
[34] B. Bradlyn, J. Cano, Z. Wang, M. Vergniory, C. Felser, R. Cava, and B. A. Bernevig, Science **353**, aaf5037 (2016).
[35] C. Herring, Physical Review **52**, 365 (1937).
[36] B. J. Wieder and C. Kane, arXiv preprint arXiv:1604.08630 (2016).
[37] D. M. Pinkerton, M. G. Banwell, and A. C. Willis, Organic Letters **11**, 4290 (2009).
[38] J.-Y. Bae, H.-J. Lee, S.-H. Youn, S.-H. Kwon, and C.-W. Cho, Organic letters **12**, 4352 (2010).

[39] L. Dong, Y.-J. Xu, L.-F. Cun, X. Cui, A.-Q. Mi, Y.-Z. Jiang, and L.-Z. Gong, Organic letters **7**, 4285 (2005).

[40] A. V. Butin, T. A. Nevolina, V. A. Shcherbinin, I. V. Trushkov, D. A. Cheshkov, and G. D. Krapivin, Organic & biomolecular chemistry **8**, 3316 (2010).

[41] D. Šterk, M. Stephan, and B. Mohar, Organic letters **8**, 5935 (2006).

[42] A. Eloi, F. Rose-Munch, E. Rose, A. Pille, P. Lesot, and P. Herson, Organometallics **29**, 3876 (2010).

[43] M. I. Aroyo, A. Kirov, C. Capillas, J. Perez-Mato, and H. Wondratschek, Acta Crystallographica Section A: Foundations of Crystallography **62**, 115 (2006).

[44] B. J. Wieder, Y. Kim, A. Rappe, and C. Kane, Physical Review Letters **116**, 186402 (2016).

[45] H. Nielsen and M. Ninomiya, Nucl. Phys. B , 20 (1981).

[46] H. Nielsen and M. Ninomiya, Nucl. Phys. B , 173 (1981).

[47] A. Bouhon and A. Black-Schaffer, (to be submitted).

[48] C. Triola, J.-X. Zhu, A. Migliori, and A. V. Balatsky, Physical Review B **92**, 045401 (2015).

[49] D. Hamann, M. Schlüter, and C. Chiang, Physical Review Letters **43**, 1494 (1979).

[50] P. E. Blöchl, Physical Review B **50**, 17953 (1994).

[51] D. Vanderbilt, Physical Review B **41**, 7892 (1990).

[52] G. Kresse and J. Hafner, Journal of Physics: Condensed Matter **6**, 8245 (1994).

[53] G. Kresse and J. Hafner, Phys. Rev. B **47**, 558 (1993).

[54] G. Kresse and J. Furthmüller, Physical Review B **54**, 11169 (1996).

[55] G. Kresse and J. Furthmüller, Computational Materials Science **6**, 15 (1996).

[56] G. Kresse and D. Joubert, Physical Review B **59**, 1758 (1999).

[57] P. Giannozzi, S. Baroni, N. Bonini, M. Calandra, R. Car, C. Cavazzoni, D. Ceresoli, G. L. Chiarotti, M. Cococcioni, I. Dabo, A. D. Corso, S. de Gironcoli, S. Fabris, G. Fratesi, R. Gebauer, U. Gerstmann, C. Gougoussis, A. Kokalj, M. Lazzeri, L. Martin-Samos, N. Marzari, F. Mauri, R. Mazzarello, S. Paolini, A. Pasquarello, L. Paulatto, C. Sbraccia, S. Scandolo, G. Sclauzero, A. P. Seitsonen, A. Smogunov, P. Umari, and R. M. Wentzcovitch, Journal of Physics: Condensed Matter **21**, 395502 (2009).

[58] J. P. Perdew, K. Burke, and M. Ernzerhof, Physical review letters **77**, 3865 (1996).

[59] A. Merkys, A. Vaitkus, J. Butkus, M. Okulič-Kazarinas, V. Kairys, and S. Gražulis, Journal of applied crystallography **49** (2016).

[60] S. Gražulis, A. Merkys, A. Vaitkus, and M. Okulič-Kazarinas, Journal of applied crystallography **48**, 85 (2015).

[61] S. Gražulis, A. Daškevič, A. Merkys, D. Chateigner, L. Lutterotti, M. Quiros, N. R. Serebryanaya, P. Moeck, R. T. Downs, and A. Le Bail, Nucleic acids research **40**, D420 (2012).

[62] S. Gražulis, D. Chateigner, R. T. Downs, A. Yokochi, M. Quirós, L. Lutterotti, E. Manakova, J. Butkus, P. Moeck, and A. Le Bail, Journal of Applied Crystallography **42**, 726 (2009).

[63] R. T. Downs and M. Hall-Wallace, American Mineralogist **88**, 247 (2003).

[64] S. P. Ong, W. D. Richards, A. Jain, G. Hautier, M. Kocher, S. Cholia, D. Gunter, V. L. Chevrier, K. A. Persson, and G. Ceder, Computational Materials Science **68**, 314 (2013).

[65] H. J. Monkhorst and J. D. Pack, Physical Review B **13**, 5188 (1976).

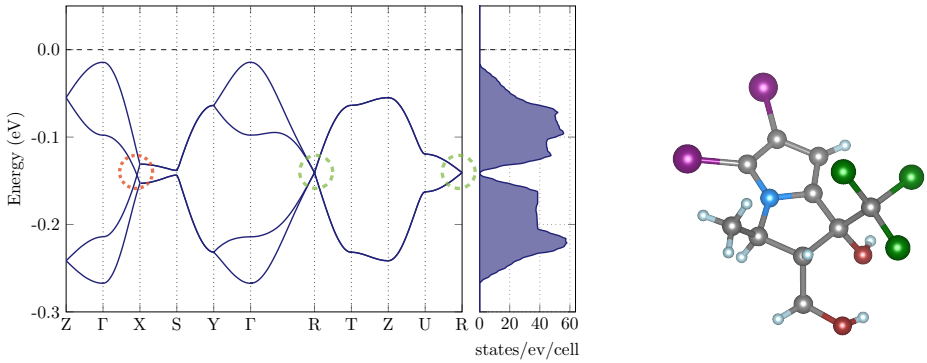

(a) $C_{10}H_{10}Br_2Cl_3NO_2$

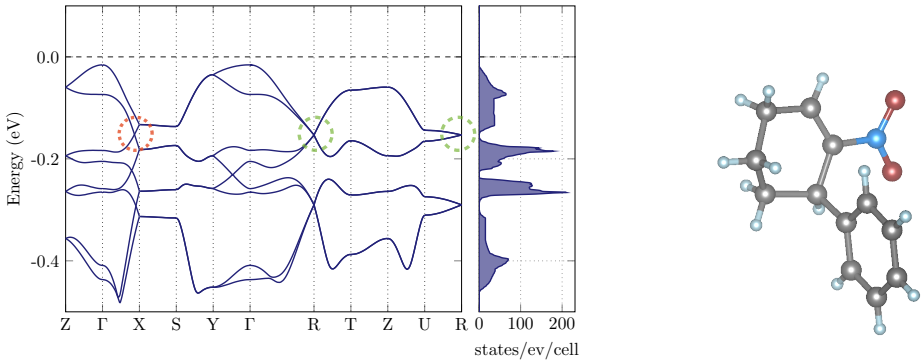

(b) $C_{12}H_{13}NO_2$

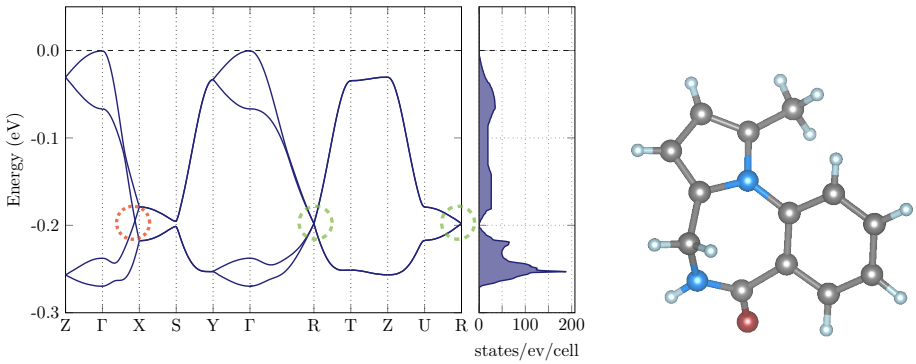

(c) $C_{13}H_{12}N_2O$

FIG. 3: **Electronic structure and molecular structure of materials with Dirac crossings in the valence band.** The colors indicate: gray: carbon, light-blue: hydrogen, blue: nitrogen, red: oxygen, purple: bromine, green: chlorine.

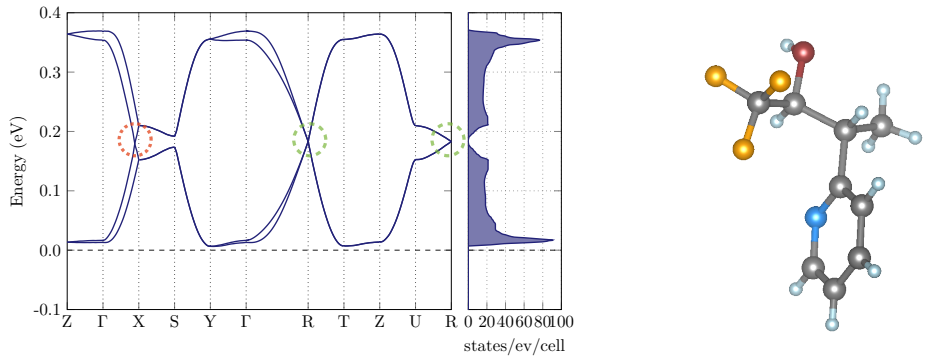

(a) $C_9H_{10}F_3NO$

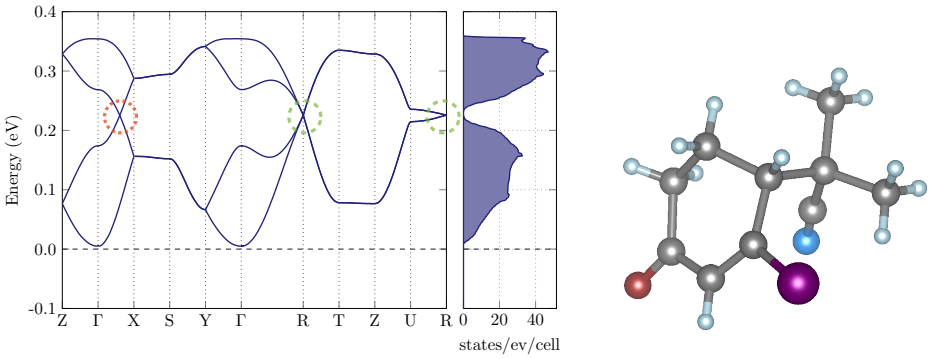

(b) $C_{10}H_{12}BrNO$

FIG. 4: **Electronic structure and molecular structure of materials with Dirac crossings in the conduction band.** The chemical elements are indicated by the colors: carbon (gray), hydrogen (light-blue), nitrogen (blue), oxygen (red), fluorine (yellow) and bromine (purple).